Author's Accepted Manuscript

Electrospun nanofiber membranes incorporating fluorosilane-coated TiO$_2$ nanocomposite for direct contact membrane distillation

Eui-Jong Lee, Alicia Kyoungjin An, Tao He, Yun Chul Woo, Ho Kyong Shon

Cite this article as: Eui-Jong Lee, Alicia Kyoungjin An, Tao He, Yun Chul Woo and Ho Kyong Shon, Electrospun nanofiber membranes incorporating fluorosilane-coated TiO$_2$ nanocomposite for direct contact membrane distillation, *Journal of Membrane Science*, http://dx.doi.org/10.1016/j.memsci.2016.07.019

Electrospun nanofiber membranes incorporating fluorosilane-coated

TiO$_2$ nanocomposite for direct contact membrane distillation

Eui-Jong Lee[1], Alicia Kyoungjin An[1*,] Tao He[2], Yun Chul Woo[3], and Ho Kyong Shon[3]

[1] School of Energy and Environment, City University of Hong Kong, Tat Chee Avenue Kowloon, Hong Kong, China

[2] Shanghai Advanced Research Institute, Chinese Academy of Sciences, No. 99 Haike Road, Pudong Shanghai, China

[3] Centre for Technology in Water and Wastewater, School of Civil and Environmental Engineering, University of Technology Sydney (UTS), P.O. Box 123, 15 Broadway, NSW 2007, Australia

[*]Corresponding author: Tel: + (852)-3442-9626, Fax: + (852)-3442-0688, E-mail: alicia.kjan@cityu.edu.hk

1

Abstract

The electrospinning technique as a method for fabricating hydrophobic membranes for membrane distillation (MD) has received much attention in recent times. In this study, TiO_2 functionalized with 1H,1H,2H,2H-perfluorooctyltriethoxysilane was added directly to the dope solution for electrospinning in order to increase the hydrophobicity of the resulting MD membranes. Three concentrations (10%, 15% and 20%) of polyvinylidene fluoride-co-hexafluoropropylene (PH) dope solution were used for electrospinning with various amounts of TiO_2 (1%, 5% and 10%) to generate nanofibers. The electrospun nanofiber membrane (ENM) of 20% PH with 10% TiO_2 exhibited the highest surface hydrophobicity (contact angle = 149°) resulting from good dispersion of the TiO_2 particles, while the highest liquid entry pressure of 194.5 kPa was observed for the ENM comprising 10% PH with 10% TiO_2 due to its reduced pore sizes. Furthermore, the ENMs containing 10% TiO_2 exhibited better flux and stable salt rejection than commercial and ENMs without TiO_2. Notably, there was no severe wetting in the 20% PH ENM with 10% TiO_2 over seven days of operation, despite the high salt concentration (7.0 wt% NaCl) of the feed water.

Keywords: Electrospun nanofiber membrane; Titanium dioxide; Membrane distillation; Superhydrophobicity; Electrospinning

1. Introduction

Membrane distillation (MD), a thermally driven separation process, allows only water vapor to pass through the pores of a hydrophobic membrane at relatively low temperature and pressure, while leaving non-volatile matter in the feed [1]. Owing to this operating mechanism, the MD

process is now emerging as a system for desalination that can not only produce high quality water (theoretically 100% rejection) without extensive pretreatment, but also reduce energy consumption by using waste heat [2], for use in applications including brine management, food and pharmaceutical processing, and wastewater treatment. Despite these advantages, however, this technology has some major disadvantages, such as low flux and wetting inside the pores of the membrane, which is accelerated by fouling or scaling, and influences both the water quality and productivity [3]. To offset these limitations, an ideal membrane for MD must enable water vapor to penetrate through the membrane easily, exhibit water-repellent properties (i.e., hydrophobicity), and have a high void ratio, lower fouling, and high chemical/thermal stability [4]. Moreover, the membrane thickness must be properly controlled in order to increase the vapor permeability and energy efficiency of the membrane, when considering heat and mass transfer.

Electrospun nanofiber membranes (ENMs) have continued to gain recognition and are of great interest due to their high void volume fraction and hydrophobicity [5]. Furthermore, the membrane structure can be controlled easily using the electrospinning method by changing the dope solution concentration, voltage, flow rate, and the distance from the collector, as well as the ambient conditions. Typically, hydrophobic polymers such as polytetrafluoroethylene (PTFE), polypropylene (PP), and polyvinylidene fluoride (PVDF) are used to fabricate MD membranes [6], though PVDF is preferred due to its solubility. Although the structure of ENMs and the inherent hydrophobicity of the polymer are effective in preventing wetting and preserving the high productivity of the membrane, many attempts have been made to improve the membrane properties [7] because the reduction of the permeability of the ENMs by wetting cannot, fundamentally, be avoided.

Pore size, distribution and geometry, hydrophobicity, and the surface energy of a membrane are all significant properties that affect membrane wetting, so their effects on the liquid entry pressure (LEP) of a membrane are well studied. A higher membrane LEP is ascribed to enhance the membrane properties towards high surface hydrophobicity and low surface energy. Among the methods for enhancing the properties of MD membranes, numerous approaches have been attempted through their surface modification with CF_4 plasma [8–10], fluoroalkylsilane [11], and hydrophobic nanoparticles [12,13]. Specifically, nanomaterials have been incorporated as versatile materials for obtaining a superhydrophobic surface with a high contact angle (>150°) and low hysteresis angle (<10°), as inspired by the extremely water-repellent surface of the lotus leaf and silver ragwort leaf. Recently, certain reports have documented hydrophobic membranes functionalized with nanomaterials for application in MD. Razmjou et al. [14] and Meng et al. [15] achieved the preparation of superhydrophobic membranes incorporating TiO_2 nanoparticles for MD using dip coating and a low temperature hydrothermal process, respectively, followed by fluorination. Although modification of the membranes enhanced their hydrophobicity, bonding of FTES to the TiO_2 coating decreased the membrane permeability due to pore restrictions [15]. Only the selective (upper) layer of the dual-layer membrane displayed remarkable hydrophobicity, and to accomplish better MD performance, a thicker selective layer was required [16]. However, thick membranes can cause high resistance to mass transfer, resulting in low permeability [17].

On the other hand, enhancement of the properties of ENMs by simple modification to increase their hydrophobicity and durability has shown promising results in MD applications. Wang et al. [13] introduced various bio-inspired approaches for achieving superhydrophobicity through post-treatment with nanoparticles or direct application of nanomaterials by electrospinning.

4

Furthermore, another group reported outstanding superhydrophobic dual-layer ENMs for direct contact membrane distillation (DCMD), where an extremely water-repellent surface of the ENMs was obtained [16,18]. Although recent studies related to hydrophobic ENMs with nanomaterials have been reported, most have focused on the surface properties of ENMs for use in short term operations [13]. Such hydrophobic modifications were primarily achieved by coating of the surface of membranes, which requires large amounts of nanoparticles [16,18]. Moreover, only limited information as to their long-term performance is available for MD nanocomposite ENMs with reference to the durability of hydrophobicity over progressive fouling, wetting, or the likelihood of nanoparticle detachment.

In this study, we set out to fabricate a robust and hydrophobic membrane for achieving enhanced MD performance by adding functionalized hydrophobic TiO_2 nanoparticles into the dope solution used for electrospinning. It was expected that the resultant protruding nanofibers would have higher hydrophobicity, which is ascribed to surface roughness, enhanced pore geometry, as well as chemical resistance to the feed solution. Inorganic nanoparticles such as Al_2O_3, SiO_2 and TiO_2 improve the electrical conductivity of polymer electrolyte, among which TiO_2 appeared to have potential for the most remarkable improvement [19]. Specifically, TiO_2 is a favorable nanomaterial as an additive due to its stability, non-toxicity, and low cost [20], and its photocatalytic activity gives it potential to enhance the antifouling properties of membrane [21,22]. Previous research have shown the applicability of TiO_2 nanoparticles as an additive for ENMs in terms of membrane fabrication for photocatalytic degradation [23–25] and air filtration [26]. However, there have been few reports related to the direct application of TiO_2 nanoparticles in ENMs for MD processes via electrospinning. In this study, various loadings of TiO_2, which was functionalized to produce a hydrophobic surface as pristine TiO_2 is hydrophilic,

5

were incorporated into a polyvinylidene fluoride-co-hexafluoropropylene (PH) solution. The effects of the hydrophobic TiO_2 particles on the properties of the ENMs were investigated, and lab-scale MD was performed with the resultant membranes to evaluate their long-term performances. Concentrate (7.0 wt% NaCl) was used as a feed solution to demonstrate the performance of these membranes without compromising durability and sustainable operation by wetting, fouling.

2. Materials and methods

2.1. Membrane material and chemicals

The dope solution for electrospinning was prepared from PVDF-HFP (referred herein as PH, M_w = 455,000 g/mol), lithium chloride (LiCl) as an additive, with N,N-dimethylformamide (DMF) and acetone as solvents, all of which were purchased from Sigma-Aldrich. Titanium dioxide (TiO_2, particle size = 21 nm) and 1H,1H,2H,2H-perfluorooctyltriethoxysilane (FTES) used in the fluorination were also purchased from Sigma-Aldrich. Commercial PVDF membrane (HVHP, 0.45 μm diameter) purchased from Millipore was used for the comparison of performance to treat concentrate in this study.

2.2. TiO_2 functionalization and dope solution preparation

To introduce the desired hydrophobic characteristics to TiO_2 nanoparticles and improve their dispersion in the PVDF dope solution, the as-received hydrophilic TiO_2 nanoparticles were functionalized using FTES. Pristine TiO_2 nanoparticles (1.6 g) were dispersed in toluene (50 mL) in a bottle using sonication for 1 h. FTES was hydroxylated by placing FTES (0.5 g) and distilled

water (0.75 g) in toluene (50 mL), and stirring the solution well for 1 h. A mixture of the two aforementioned solutions was stirred in a glove box filled with N_2 gas for 18 h to allow the FTES to bond with the TiO_2 particles, as shown in Fig. 1. After covalent bonding of the TiO_2 particles with FTES was complete, the modified particles were thoroughly washed with toluene and dried in an oven at 60°C for 48 h. The as-prepared FTES-TiO_2 particles were then mixed well in DMF and sonicated for 2 h, prior to their addition to the dope solutions.

Fig. 1. Schematic representation of functionalized TiO_2 with FTES

A predetermined weight of PH polymer was added to DMF with a small amount of LiCl additive (0.005 wt%) to prepare dope solutions with 15% and 20% PH, while acetone/DMF (40/60 wt%) was used for stable fiber formation in the case of the 10% PH solution due to low concentration of dope solution [26,27]. After complete dissolution of the polymer over the course of one day, the as-prepared hydrophobic TiO_2 (1%, 5%, and 10%) was combined with each of the aforementioned PH solutions (10%, 15%, and 20%). The mixtures were stirred at 50 °C for one day, and then gently agitated at ambient temperature (25 °C) for 4 h before electrospinning was performed.

2.3. Fabrication of ENMs

The electrospinner used in this study was comprised of a plastic syringe combined with a metal nozzle and a grounded rotating collector covered with aluminum foil. The flow rate of the addition of the dope solution by syringe was controlled by syringe pump, and the metal nozzle

7

(0.5/0.8 mm inner/outer diameters) was linked to a high voltage (18 kV) supplier to provide a positive charge to the dope solution for the nanofibers flying to the collector, which was placed 15 cm from the nozzle. During electrospinning, the positively charged dope solution flew to the collector, moving at a velocity of 10 mm/s from left end to right end. The syringe pump operated at a flow rate of 1.0 mL/h at 25 °C and 55% humidity. In order to eliminate the residual solvent in the membrane, the ENM was dried completely at 60 °C for 24 h in a conventional oven.

2.4. Characterization of PH-TiO$_2$ ENMs

2.4.1. Verification of functionalized TiO$_2$ nanoparticles and ENM

To investigate and compare the chemical bonds between pristine and functionalized TiO$_2$, Fourier transform infrared spectroscopy (FTIR) analysis was conducted (IRAffinity-1 FTIR spectrometer, Shimadzu). X-ray diffractometer (X'Pert^3 Powder, PANalytical, Netherlands) using Cu Kα radiation was used at the condition of 40 kV and 40 mA to confirm TiO$_2$ embedded in ENM. The sample was scanned from 10° to 70° at the scan rate of 10°/min.

2.4.2. Pore size distribution, liquid entry pressure (LEP), and contact angle measurements

A capillary flow porometer (POROLUX^{TM}1000, Germany) was used to measure the pore size distribution, as well as the mean and maximum pore sizes of the membranes prepared. The membrane was wetted with a low surface tension liquid (POROFIL, 16 mN/m) and placed in a sealed chamber that was then pressurized with N$_2$ gas. After first bubble point, when the pressure was high enough to push the liquid out from the largest pore, the gas flow was increased at a fluctuating rate until all of the pores were opened. This process was discontinued after a linear increase of the gas flow was observed. After completion of the wet curve recording process, a similar process was implemented to acquire the dry curve until the linear dry curve intersected

the linear section at the end of the wet curve. The pore size could be determined using the program's automatic calculation based on the bubble point and gas permeation.

LEP was measured using the same capillary flow porometer. After placing the membrane sample in a sealed chamber, sufficient distilled water was poured on the surface of the membrane to cover the membrane completely. The water on the surface of the membrane was pushed into the membrane by the N_2 gas as the pressure was increased gradually at a rate of 0.16 kPa/s. When the pressure was sufficiently high to enable penetration of water through the membrane, the pressure was not increased any further, which resulted in a pressure drop. The pressure value at the point immediately prior to the pressure drop is regarded as the LEP, and to reduce any error, this measurement was repeated more than three times.

The EASYDROP Contact Angle Measuring System (Kruss, Germany) was used to measure contact angles of water on the membrane surface. A membrane specimen was placed on a sample board, and a 5 µL droplet of deionized water was placed on the membrane using a syringe equipped with a thin needle. The image captured of the water drop on the membrane was transferred to a computer equipped with a video-digitizer board and shown on the monitor. DSA1 software was used to analyze the image and calculate the contact angle by a geometrical method (sessile drop).

2.4.3. Porosity and tensile strength measurement

The membrane porosity was determined by a gravimetric method. After measuring the weight of the dry membrane sample (3 cm $\times$ 3 cm), the sample was fully wetted with ethanol and the weight of the wetted membrane was measured after 30 min. The porosity could be measured by

calculating the volume of ethanol in the membrane sample from the dry weight, wet weight, and material density of ethanol and the PH polymer.

The tensile strength of each membrane sample was measured using a Materials Testing Machine (LS1, Lloyd-ametek) with a 1 kN load cell. After measuring the thickness of the sample (1 cm × 3 cm) by digital micrometer (Mitutoyo, Japan), the test was carried out at an elongation rate of 5 mm/min at room temperature.

2.4.4. Morphology and diameter of the nanofibers

The morphology of the membrane was visualized by scanning electron microscopy (SEM). The ENMs were coated with a thin layer of gold by sputtering for 80 s to obtain a clear surface image. The coated membrane was analyzed with an EVO MA 10 (Zeiss, Germany) scanning electron microscope at an accelerating voltage of 20 kV. The diameter of the fibers was determined from the SEM images using the software program ImageJ. After setting the scale between the pixels and the real distance, one hundred fibers were measured manually without duplication of any fiber. Transmission electron microscopy (TEM) (Philips CM 20) was performed with an acceleration voltage of 200 kV to observe dispersion and position of TiO_2 particles.

2.5. Direct contact membrane distillation (DCMD) experiment

Evaluation of the performances of the ENMs in DCMD was conducted with a lab-scale DCMD system (Fig. 2) composed of pumps, a feed/permeate tank, digital balance, flow meter, and custom-made acrylic casing. The feed and permeate solutions were circulated in opposite directions across the hydrophobic membrane (9.8 cm^2) mounted in the acrylic casing. The hot feed water, with a conductivity of around 115 μS/cm (7.0 wt% NaCl), was heated in the range of 60~61 °C by the hotplate/stirrer, and circulated at a flow rate of 450 mL/min. The cold permeate

10

water, with a conductivity of below 2 µS/cm, was circulated at the same flow rate while keeping

the temperature at approximately 20 °C. The permeate tank filled with 1 L of distilled water was

placed on the digital balance connected to the computer for data logging. The conductivity probe

was submerged in the permeate solution to monitor the conductivity and temperature. All of the

tubes used in the experiment were covered with an insulator to minimize heat loss, and the flux

data and permeate water conditions were recorded by a computer and conductivity meter,

respectively.

Fig. 2. Schematic diagram of the lab-scale DCMD system

3. Results and discussion

3.1 Evidence of functionalized TiO_2 embedded in ENM

Figure 3 shows the FTIR spectra of FTES, neat TiO_2 particles, and TiO_2 particles functionalized

with FTES. Both pristine and modified TiO_2 exhibited broad absorption bands between 440 and

890 cm^{-1}, where the peaks at 460 and 820 (763) cm^{-1} were attributed to the Ti–O stretching

vibration [27] and Ti–O–Ti bonds [28], respectively. Another broad absorption band and a sharp

peak derived from physically adsorbed water on the surface of TiO_2 were also observed around

3400 and 1620 cm^{-1}, respectively [29]. The original spectral features of TiO_2 could thus be

identified in the profiles of both the untreated and treated TiO_2 particles. However, several peaks

assignable to $v(C-F_2)$ could also be observed at 1273, 1191, 1134, and 1111 cm^{-1} in the FTIR

spectra of FTES and functionalized TiO_2 [30]. Moreover, the peaks in the range of 1110 to 1350

11

cm^{-1} and those at 820 and 890 cm^{-1} were ascribed to ν(C–F$_3$) [30], where it was difficult to distinguish the ν(C-F$_3$) absorption bands due to their overlap with the Ti–O–Ti band in the case of functionalized TiO$_2$ [29]. It can thus be confirmed that the hydrophilic surface of pristine TiO$_2$ was successfully modified with FTES to form hydrophobic particles. The hydrophobicity of the particles prepared could also be confirmed by their insolubility in water, as shown in the below photo (Fig. 3(d)).

Fig. 3. FTIR spectra of (a) FTES, (b) pristine TiO$_2$ nanoparticles, and (c) functionalized TiO$_2$ nanoparticles. (d) Immiscible modified TiO$_2$ particles in distilled water.

The X-ray diffraction showed two types of PVDF polymorphs (α and β phase) in both neat PH ENM and PH ENM incorporated with TiO$_2$ particles (Fig. 4). A diffraction peak at 18.5° is attributed to the (020) reflection of the α phase [31]. In the case of β phase, two diffraction peaks at 20.7° and 36.4° were observed, the former of which is the strong peak corresponding to the (110) and (200) reflections, and the latter of which is the weak peak corresponding to the (201) reflection [32]. While the addition of TiO$_2$ caused a slight decrease in the β phase, the PH ENM containing TiO$_2$ still shows a similar spectrum whereby the β phase is more intense than the α phase. Additional diffraction peaks were observed at 25.4° and 48.2°, corresponding to the characteristic peaks of TiO$_2$ [33], which confirms the successful introduction of TiO$_2$ particles into the PH fibers.

Fig. 4. X-ray diffraction patterns of (a) neat 20% PH ENM and (b) 20% PH ENM containing 10% functionalized TiO$_2$ nanoparticles.

3.2 Surface morphology of ENMs

Prior studies show that an even and uniform distribution of nanocomposites in a nanofiber is important when nanoparticles are added to a polymer solution in order to improve the properties and performance of the resulting membrane [34]. Lalia et al. [35] reported that the incorporation of nanocrystalline cellulose (NCC) at concentrations of 1~4% into nanofibers could be achieved without the formation of beads in 10% PH solution; therefore, in this study, 1%, 5%, and 10% TiO$_2$ particles were incorporated into the nanofibers, because higher than 10% concentrations induced the formation of abnormal beads that resulted in unstable nanofibers.

In all membranes, noticeable and protruding TiO$_2$ particles were observed on the surface of fibers and membranes containing more than 5% TiO$_2$ concentration. The morphology of the electrospun membranes containing 10% of TiO$_2$ particles showed the highest contact angles for each polymer concentration, as shown in the FE-SEM images presented in Fig. 5. Each fiber exhibited a unique PH concentration related morphology. While large-sized TiO$_2$ aggregates were observed in the fiber of the 15% PH ENM (Fig. 5(c)), the TiO$_2$ particles in the 10% and 20% PH showed better dispersion with evenly incorporated particles. Although the particles in the dope solution were exposed to vigorous stirring and sonication for dispersion, there was still a strong tendency for re-agglomeration among the TiO$_2$ nanoparticles during the preparation for and execution of electrospinning due to their large surface area [36]. As the TiO$_2$ concentration

13

was based on weight of polymer, the dope solution for the 10% PH ENM contained the smallest amount of TiO_2 particles per volume and thus showed the longest distance among the TiO_2 particles. The weakened influence of the Van der Waals force (the dominant force affecting two molecules within a certain distance) due to the longer distance between particles explains why 10% PH can be most favorable TiO_2 particles dispersion. However, this same explanation cannot fully explicate why particle dispersion in 20% PH was better than that of the 15% PH. Nguyen et al. [37] reported that the viscosity of the solution does not affect the final size of the clusters formed during the sonication for particle dispersion. Thus, the results gained for 15% and 20% PH ENMs can be attributed to the influence of viscosity on the Brownian motion after sonication. The nanoparticles dispersed in the solution are attracted to each other due to their Brownian motion; however, higher viscosity acts as a barrier for the nanoparticles' Brownian motion. Low Brownian motion leads to lower possibility of attraction or contact among the nanoparticles, which were dispersed through sonication, and thus, lessens the re-aggregation due to the Van der Waals force [38]. Therefore, despite the larger amount of TiO_2 particles per volume in the 20% PH ENM, its higher viscosity of the dope solution led to less clusters compared to the 15% PH ENMS. Overall, the best viscosity and dispersion for higher membrane performance was found in 20% PH ENM with 10% TiO_2 concentration.

Even though well incorporated particles were observed in 10% and 20% of PH ENMs, more TiO_2 particles were apparent on the surface of the nanofibers of the latter (Fig. 5(d)) compared to that of 10% PH (Fig. 5(b)), because an appropriate time is required to position the particles on the outside of the nanofibers. When a highly volatile solvent, such as acetone, is used, the surface of the nanofibers can solidify quickly while the fluid jet is flying to the collector, whereby it becomes difficult for the particles to be transferred from the core to the shell of the nanofibers

14

[39]. As mentioned above, although nanoparticles could definitely be observed on the surface of the nanofibers in previous reports that employed only DMF [23,40], which is a less volatile solvent, surface modification of the nanocomposite was not obvious when a DMF and acetone solvent mixture was employed [41]. The protrusions and valleys resulting from the nanoparticles increase the surface hydrophobicity by mitigating wetting and reducing the water-membrane contact area [18]. Micro-wrinkles, which are attributed to buckling instabilities and contraction mismatch of the polymer solution jet [42], could be observed on the nanofiber surface of ENMs both with and without TiO_2 particles. In particular, the 20% PH ENM fiber presented an obviously wrinkled surface topography when compared to other ENMs. The effects of the hydrophobic nanoparticles are described in the MD of the concentrates presented in Sec. 3.5.

Fig. 5. FE-SEM images of (a) neat 20% PH ENM, (b) 10% PH ENM with 10% TiO_2, (c) 15% PH ENM with 10% TiO_2, and (d) 20% PH ENM with 10% TiO_2.

3.3 Nanofiber diameter and membrane pore configuration

Polymer concentration is one of the most important parameters that influence solution viscosity, which in turn affects the ability to maintain a stable nanofiber shape. As previously reported [43], as well as in this study, the diameter of the nanofibers obtained also increased with increasing PH concentration, as shown in Fig. 6. When TiO_2 particles were incorporated into the nanofibers, their diameters decreased, although the overall diameter distribution remained similar. It has also been reported, however, that fiber diameters increase upon the addition of clay nanoparticles, due to an increase in the viscosity of the polymer solution [41]. The results obtained herein can be

15

ascribed to the effects of the second electrospinning step, which involves adjacent nanofibers containing inorganic nanoparticles with higher electronic densities [44].

Pore size and distribution are critical parameters that affect the performance of nanofibers in the MD process [45]. Previous reports suggest that membranes for MD should have appropriate pore sizes to prevent wetting, as well as enhance Knudsen diffusion and viscous flow [46]. As shown in Table 1, the mean pore size of the 20% PH ENM containing TiO_2 particles was slightly lower than that of neat 20% PH ENM (0.7 µm), while the pore sizes of the 10% and 15% PH ENMs decreased to around 0.3 and 0.6 µm, respectively. These observations are due to changes in fiber diameter resulting from differences in the polymer concentration and resulting aggregation of the TiO_2 particles. Moreover, a narrow pore size distribution was observed upon decreases in the concentration of PH for 10% TiO_2 PH ENM (Fig. 7). The difference in pore size of the 10% and 15% PH ENMs in spite of the similarity of their fiber diameter can be likely attributed to the differences in solvent volatility and electrospinning time.

Fig. 6. Fiber diameter distributions of (a) neat 20% PH ENM, (b) 10% PH ENM with 10% TiO_2, (c) 15% PH ENM with 10% TiO_2, and (d) 20% PH ENM with 10% TiO_2.

Fig. 7. Pore size distributions of the neat PH ENM and PH ENMs containing TiO_2 nanoparticles.

Table 1. Properties of PH ENMs incorporating TiO_2 nanoparticles

16

3.4 Membrane hydrophobicity determined by contact angle and LEP

As shown in Table 1, the contact angles of the ENMs prepared in this study were greater than 140°, which is significantly higher than those of commercial membranes. In all membranes incorporated TiO_2 particles, the value of the contact angles were increased as the morphology of the fibers were modified through the addition of TiO_2. However, in low concentrations of TiO_2 (1% and 5%), improvement of the contact angle was marginal compared to the addition of 10% TiO_2.

Previous studies have reported the achievement of contact angles greater than 150°, i.e. so-called superhydrophobic membranes, by means of dip coating and post-treatment [14,15], or membrane surface coating [16] using nanoparticles. In this present study, electrospinning of the polymer solution containing hydrophobic nanoparticles enabled the nanoparticles to be effectively embedded on the surface of the fibers and the highest contact angle for the membrane with 20% PH and 10% TiO_2 was very close to 150° (Fig. 8(a)). Although the hydrophobicity of the surface is effectively repellent to water, water vapor keeps passing through the membrane in MD processes and there is no resistant barrier if water penetrates through the hydrophobic surface due to fouling and wetting. It is expected that not only hydrophobic surface of membrane but also hydrophobic particles embedded inside of the membrane can endure to prevent wetting.

Based on the Cantor-Laplace equation, the LEP of a porous membrane is proportional to the contact angle, liquid surface tension, and the inverse of the maximum pore size [47]:

$$LEP = \frac{-2B\gamma\cos\theta}{r_{max}} \qquad (1)$$

17

where, B and r are the shape factor and the radius of the membrane pore, respectively, γ is the surface tension of the wetting liquid, and θ represents the contact angle between the membrane sample and the wetting liquid.

Figure 8(b) shows the relationship between LEP and the inverse of the maximum pore size. As expected, LEP increased as the maximum pore size decreased. Although the 20% PH ENMs with TiO_2 particles have similar maximum pore sizes to those of neat ENM, the LEP values determined were 15 to 30 kPa higher than those of the neat ENMs. Furthermore, the ENMs (M-3, 5, 6, 9) containing higher concentrations of TiO_2 marked with black points in Figure 8(b), were located above the regression line. These results indicate that functionalized TiO_2 particles are sufficient in repelling water from the membrane due to the hydrophobicity of the nanoparticles and subsequent nanofiber modification.

Fig. 8. (a) Contact angles, and (b) LEP of ENMs incorporating TiO_2 nanoparticles.

3.5 Structural stability and porosity

The tensile strength of ENMs is closely related to the inherent mechanical properties of polymer nanofibers, as well as the structures between nanofibers [48]. Tensile strength decreases with decreases in polymer concentration, due to the fact that a low concentration of the polymer induces the formation of small diameter fibers, as has been previously reported [49]. In Table 1, the insignificant differences between the fiber diameters and tensile strengths of the 10% and 15% PH ENMs are attributed to the different solvents, whereby the accelerated evaporation of acetone

18

influenced fiber formation such that similar fiber diameters and tensile strengths were observed. Compared to neat ENM, the strength and elongation of the ENMs containing TiO$_2$ decreased slightly. Notably, the elongation of the 10% and 15% PH ENMs declined considerably, which implied a relative brittleness of the PH matrix upon the introduction of TiO$_2$ particles. The mechanical strength of all the membranes was sufficient for application in MD processes. The ENMs containing nanoparticles fabricated in this study also exhibited high porosities of around 90% (Table 1). The embedded nanoparticles in the fibers cause a slight increase in porosity, which might be attributed to the fact that protrusions of the nanoparticles on the surface of the fibers can lead to the formation of a loose structure between thin layers comprising numerous nanofibers and increased pore size.

3.6 Performance of DCMD process for desalination of concentrates

Figure 9 shows the continuous DCMD performance over two days on the desalination of an aqueous concentrate of 7.0 wt% NaCl solution using a 0.45 μm commercial PVDF membrane, as well as two PH ENMs (neat 20% PH ENM and 10% PH ENM with 10% TiO$_2$,). The MD operation was extended over a week with 20% PH ENM 10% TiO$_2$ to monitor its long-term stable performance. The commercial PVDF membrane showed the lowest initial flux of around 25 L/m^2/h, which decreased gradually during the DCMD process in combination with concomitant deterioration of the permeate water. The sharp increase in conductivity observed after 20 h indicates complete membrane wetting, most likely resulting from the inner disconnected pore structure and low porosity of the membrane. The PH ENMs prepared in this study, however, showed high fluxes of 40 L/m^2/h due to their high porosity, large pore size, and interconnected porous structure. Moreover, the permeate waters exhibited considerably stable

19

and low permeate conductivities due to their relatively high LEP prevents membrane wetting as well as high contact angle with the membranes. Neat ENM, which has an inadequate hydrophobicity, showed a gradual increase in permeate conductivity after 32 h, as well as slight decrease in flux, probably as a result of partial membrane wetting.

Interestingly, the ENMs with hydrophobic 10% TiO_2 nanoparticles embedded on the fiber surface showed low permeate conductivities (below 2.1 µS/cm for two days, and below 7.0 µS/cm for seven days), although the membranes had large pore size compared to commercial PVDF membranes. This result can be attributed to the specific structure of the ENMs composed of overlapping nanofibers surrounded by hydrophobic particles, which confers greater hydrophobicity to the entire membrane by integral modification. In addition, there was no evident change in flux over two days of MD operation in the case of the ENM comprising 20% PH with 10% TiO_2, whereas a slight decrease in flux was observed for the ENM comprising 10% PH with 10% TiO_2.

As mentioned in Section 3.2, 20% PH with 10% TiO_2 exhibited more TiO_2 particles on its surface and an obvious wrinkled structure of its fibers than did that of 10% PH with 10% TiO_2. Such a wrinkled structure is typically resistant to pore wetting, which causes a decrease in permeability during MD. In addition, this surface morphology increases the effective surface area of the membrane for the generation of more water vapor, and may reduce the temperature polarization by turbulence on the membrane surface [50]. Therefore, the unique morphology of 20% PH with 10% TiO_2 is more favorable for anti-wetting, as well as long-term MD performance. As shown in Fig. 9 (d), the permeate quality of 20% PH ENM with 10% TiO_2 during seven days did not deteriorate as dramatically as that of neat ENM in the absence of TiO_2.

20

Fig. 9. DCMD performance of (a) commercial PVDF (0.45 μm), (b) neat 20% PH ENM, (c) 10% PH ENM with 10% TiO$_2$, and (d) 20% PH ENM with 10% TiO$_2$.

In general, the addition of nano-filler to improve ENM performance was carried out using two methods, one that covers the surface of pure ENMs with polymer containing nano-fillers by electrospraying or electrospinning, and the other that electrospins the polymer solution containing the nano-fillers, as was employed in this study. Table 2 compared our study and previous literatures dealing with both pure ENMs and nano-filler added ENMs summaries information on membrane properties and MD performance. There was no significant improvement in MD performance in terms of flux, despite the fact that surface coating of nano-fillers improved the hydrophobicity of the membrane surface more dramatically than that of a mixed nano-filler and dope solution. Notwithstanding the lower surface hydrophobicity of the membranes prepared in this study using the latter method, a high flux and complete hydrophobic membrane structure was instead achieved, such that the ENM membrane inside was as hydrophobic as its surface.

Table 2. Properties and DCMD performances of neat ENMs and ENMs incorporated with nano-filler. Feed/permeate temperatures: 60/20°C; 3.5wt% NaCl feed solutions, except for PH and 10% TiO$_2$-PH (7.0 wt%).

Table 2. Properties and DCMD performance between neat ENMs and ENMs incorporated with nano-filler. Feed/permeate temperature: 60/20°C. 3.5 wt% NaCl feed solutions except for our study (7.0 wt%)

21

4. Conclusions

The integral modification of ENMs, that is, the direct addition of TiO_2 nanoparticles into the dope solution used for membrane fabrication via electrospinning, can effectively improve the hydrophobicity of the membranes prepared. While the TiO_2 particles caused a reduction in the membrane pore size due to a decrease in the fiber size, other properties, i.e., porosity, contact angle, and LEP, which are directly correlated to the MD performance, increased. The highest LEP of 194.5 kPa was obtained for a membrane comprising 10% PH with 10% TiO_2, and the largest contact angle of 149° was obtained for a membrane comprising 20% PH with 10% TiO_2. Even when the same concentration of TiO_2 was incorporated into the membranes, the morphology of the TiO_2 on the fiber surfaces was dependent on the polymer concentration, particle mass, and volatility of the solvent. The particles on the fiber surface could confer hydrophobicity to the entire membrane, as opposed to only its surface, which prevented the deterioration of the quality of the permeate water during membrane operation over two days. Notably, the membrane comprising 20% PH with 10% TiO_2 exhibited a flux of approximately 40 $L/m^2/h$ without any noticeable decrease in its permeability, even over operation of seven days.

References

[1]   Y.C. Woo, Y. Kim, W.-G. Shim, L.D. Tijing, M. Yao, L.D. Nghiem, et al.,
       Graphene/PVDF flat-sheet membrane for the treatment of RO brine from coal seam gas
       produced water by air gap membrane distillation, J. Memb. Sci. 513 (2016) 74–84.
       doi:10.1016/j.memsci.2016.04.014.

[2]   M. Qtaishat, M. Khayet, T. Matsuura, Novel porous composite hydrophobic/hydrophilic
       polysulfone membranes for desalination by direct contact membrane distillation, J. Memb.
       Sci. 341 (2009) 139–148. doi:10.1016/j.memsci.2009.05.053.

[3]   C.-Y. Kuo, H.-N. Lin, H.-A. Tsai, D.-M. Wang, J.-Y. Lai, Fabrication of a high
       hydrophobic PVDF membrane via nonsolvent induced phase separation, Desalination. 233
       (2008) 40–47. doi:10.1016/j.desal.2007.09.025.

[4]   S. Bonyadi, T.S. Chung, Flux enhancement in membrane distillation by fabrication of dual
       layer hydrophilic–hydrophobic hollow fiber membranes, J. Memb. Sci. 306 (2007) 134–
       146. doi:10.1016/j.memsci.2007.08.034.

[5]   Y.C. Woo, L.D. Tijing, M.J. Park, M. Yao, J.-S. Choi, S. Lee, et al., Electrospun dual-
       layer nonwoven membrane for desalination by air gap membrane distillation, Desalination.
       (2015). doi:10.1016/j.desal.2015.09.009.

[6]   E. Drioli, A. Ali, F. Macedonio, Membrane distillation: Recent developments and
       perspectives, Desalination. 356 (2015) 56–84. doi:10.1016/j.desal.2014.10.028.

[7]   F.E. Ahmed, B.S. Lalia, R. Hashaikeh, A review on electrospinning for membrane
       fabrication : Challenges and applications, Des. 356 (2014) 15–30.
       doi:10.1016/j.desal.2014.09.033.

[8]   X. Wei, B. Zhao, X.M. Li, Z. Wang, B.Q. He, T. He, et al., CF 4 plasma surface
       modification of asymmetric hydrophilic polyethersulfone membranes for direct contact
       membrane distillation, J. Memb. Sci. 407-408 (2012) 164–175.
       doi:10.1016/j.memsci.2012.03.031.

[9]   C. Yang, M. Tian, Y. Xie, X.-M. Li, B. Zhao, T. He, et al., Effective evaporation of CF4
       plasma modified PVDF membranes in direct contact membrane distillation, J. Memb. Sci.
       482 (2015) 25–32. doi:10.1016/j.memsci.2015.01.059.

[10]   M. Tian, Y. Yin, C. Yang, B. Zhao, J. Song, J. Liu, et al., CF4 plasma modified highly
       interconnective porous polysulfone membranes for direct contact membrane distillation
       (DCMD), Desalination. 369 (2015) 105–114. doi:10.1016/j.desal.2015.05.002.

[11]   H. Fang, J.F. Gao, H.T. Wang, C.S. Chen, Hydrophobic porous alumina hollow fiber for
       water desalination via membrane distillation process, J. Memb. Sci. 403-404 (2012) 41–46.
       doi:10.1016/j.memsci.2012.02.011.

[12]   J. Zhang, Z. Song, B. Li, Q. Wang, S. Wang, Fabrication and characterization of
       superhydrophobic poly (vinylidene fluoride) membrane for direct contact membrane
       distillation, Desalination. 324 (2013) 1–9. doi:10.1016/j.desal.2013.05.018.

[13]   X. Wang, B. Ding, J. Yu, M. Wang, Engineering biomimetic superhydrophobic surfaces
       of electrospun nanomaterials, Nano Today. 6 (2011) 510–530.

doi:10.1016/j.nantod.2011.08.004.

[14] A. Razmjou, E. Arifin, G. Dong, J. Mansouri, V. Chen, Superhydrophobic modification of TiO 2 nanocomposite PVDF membranes for applications in membrane distillation, J. Memb. Sci. 415-416 (2012) 850–863. doi:10.1016/j.memsci.2012.06.004.

[15] S. Meng, J. Mansouri, Y. Ye, V. Chen, Effect of templating agents on the properties and membrane distillation performance of TiO2-coated PVDF membranes, J. Memb. Sci. 450 (2014) 48–59. doi:10.1016/j.memsci.2013.08.036.

[16] Y. Liao, C.-H. Loh, R. Wang, T. Fane, Electrospun superhydrophobic membranes with unique structures for membrane distillation., ACS Appl. Mater. Interfaces. (2014). doi:10.1021/am503968n.

[17] M.S. El-Bourawi, Z. Ding, R. Ma, M. Khayet, A framework for better understanding membrane distillation separation process, J. Memb. Sci. 285 (2006) 4–29. doi:10.1016/j.memsci.2006.08.002.

[18] Y. Liao, R. Wang, A.G. Fane, Fabrication of bioinspired composite nanofiber membranes with robust superhydrophobicity for direct contact membrane distillation, Environ. Sci. Technol. 48 (2014) 6335–6341. doi:10.1021/es405795s.

[19] S.H. Chung, Y. Wang, L. Persi, F. Croce, S.G. Greenbaum, B. Scrosati, et al., Enhancement of ion transport in polymer electrolytes by addition of nanoscale inorganic oxides, J. Power Sources. 97-98 (2001) 644–648. doi:10.1016/S0378-7753(01)00748-0.

[20] K. Nagaveni, G. Sivalingam, M.S. Hegde, G. Madras, Photocatalytic Degradation of Organic Compounds over Combustion-Synthesized Nano-TiO2, Environ. Sci. Technol. 38 (2004) 1600–1604. doi:10.1021/es034696i.

[21] S.S. Madaeni, S. Zinadini, V. Vatanpour, A new approach to improve antifouling property of PVDF membrane using in situ polymerization of PAA functionalized TiO2 nanoparticles, J. Memb. Sci. 380 (2011) 155–162. doi:10.1016/j.memsci.2011.07.006.

[22] S.S. Madaeni, N. Ghaemi, Characterization of self-cleaning RO membranes coated with TiO2 particles under UV irradiation, J. Memb. Sci. 303 (2007) 221–233. doi:10.1016/j.memsci.2007.07.017.

[23] J.S. Im, M. Il Kim, Y.-S. Lee, Preparation of PAN-based electrospun nanofiber webs containing TiO2 for photocatalytic degradation, Mater. Lett. 62 (2008) 3652–3655. doi:10.1016/j.matlet.2008.04.019.

[24] N. Daels, M. Radoicic, M. Radetic, K. De Clerck, S.W.H. Van Hulle, Electrospun nanofibre membranes functionalised with TiO2 nanoparticles: Evaluation of humic acid and bacterial removal from polluted water, Sep. Purif. Technol. 149 (2015) 488–494. doi:10.1016/j.seppur.2015.06.016.

[25] N. Daels, M. Radoicic, M. Radetic, S.W.H. Van Hulle, K. De Clerck, Functionalisation of electrospun polymer nanofibre membranes with TiO 2 nanoparticles in view of dissolved organic matter photodegradation, Sep. Purif. Technol. 133 (2014) 282–290. doi:10.1016/j.seppur.2014.06.040.

[26]   H. Wan, N. Wang, J. Yang, Y. Si, K. Chen, B. Ding, et al., Hierarchically structured polysulfone/titania fibrous membranes with enhanced air filtration performance, J. Colloid Interface Sci. 417 (2014) 18–26. doi:10.1016/j.jcis.2013.11.009.

[27]   Y. Zhao, L. Xu, Y. Wang, C. Gao, D. Liu, Preparation of Ti-Si mixed oxides by sol-gel one step hydrolysis, Catal. Today. 93-95 (2004) 583–588. doi:10.1016/j.cattod.2004.06.124.

[28]   V. a. Zeitler, C. a. Brown, a Brown, The Infrared Spectra of Some Ti-O-Si, Ti-O-Ti and Si-O-Si Compounds, J. Phys. Chem. 61 (1957) 1174–1177. doi:10.1021/j150555a010.

[29]   S. Pazokifard, S.M. Mirabedini, M. Esfandeh, S. Farrokhpay, Fluoroalkylsilane treatment of TiO 2 nanoparticles in difference pH values: Characterization and mechanism, Adv. Powder Technol. 23 (2012) 428–436. doi:10.1016/j.apt.2012.02.006.

[30]   E. da C. Mattos, E.D. Moreira, M.F. Diniz, R.C.L. Dutra, G. da Silva, K. Iha, et al., Characterization of polymer-coated RDX and HMX particles, Propellants, Explos., Pyrotech. 33 (2008) 44–50. doi:10.1002/prep.200800207.

[31]   W.A. Yee, S. Xiong, G. Ding, C.A. Nguyen, P.S. Lee, J. Ma, et al., Supercritical carbon dioxide-treated electrospun poly(vinylidene fluoride) nanofibrous membranes: Morphology, structures and properties as an ionic-liquid host, Macromol. Rapid Commun. 31 (2010) 1779–1784. doi:10.1002/marc.201000201.

[32]   Y.-J. Kim, C.H. Ahn, M.B. Lee, M.-S. Choi, Characteristics of electrospun PVDF/SiO2 composite nanofiber membranes as polymer electrolyte, Mater. Chem. Phys. 127 (2011) 137–142. doi:http://dx.doi.org/10.1016/j.matchemphys.2011.01.046.

[33]   W.W. Cui, D.Y. Tang, Z.L. Gong, Electrospun poly(vinylidene fluoride)/poly(methyl methacrylate) grafted TiO 2 composite nanofibrous membrane as polymer electrolyte for lithium-ion batteries, J. Power Sources. 223 (2013) 206–213. doi:10.1016/j.jpowsour.2012.09.049.

[34]   L.D. Tijing, J.S. Choi, S. Lee, S.H. Kim, H.K. Shon, Recent progress of membrane distillation using electrospun nanofibrous membrane, J. Memb. Sci. 453 (2014) 435–462. doi:10.1016/j.memsci.2013.11.022.

[35]   B.S. Lalia, E. Guillen, H.A. Arafat, R. Hashaikeh, Nanocrystalline cellulose reinforced PVDF-HFP membranes for membrane distillation application, Desalination. 332 (2014) 134–141. doi:10.1016/j.desal.2013.10.030.

[36]   S.H. Othman, S. Abdul Rashid, T.I. Mohd Ghazi, N. Abdullah, Dispersion and stabilization of photocatalytic TiO 2 nanoparticles in aqueous suspension for coatings applications, J. Nanomater. 2012 (2012). doi:10.1155/2012/718214.

[37]   V.S. Nguyen, D. Rouxel, B. Vincent, Dispersion of nanoparticles: From organic solvents to polymer solutions, Ultrason. Sonochem. 21 (2014) 149–153. doi:10.1016/j.ultsonch.2013.07.015.

[38]   T. Tadano, R. Zhu, Y. Muroga, T. Hoshi, D. Sasaki, S. Yano, et al., A new mechanism for the silica nanoparticle dispersion–agglomeration transition in a poly(methyl

methacrylate)/silica hybrid suspension, 46 (2014) 1–7. doi:10.1038/pj.2014.6.

[39]   B. Ding, J. Lin, X. Wang, J. Yu, J. Yang, Y. Cai, Investigation of silica nanoparticle distribution in nanoporous polystyrene fibers, Soft Matter. 7 (2011) 8376–8383. doi:10.1039/C1SM05791J.

[40]   Y.J. Kim, C.H. Ahn, M.B. Lee, M.S. Choi, Characteristics of electrospun PVDF/SiO\n 2 composite nanofiber membranes as polymer electrolyte, Mater. Chem. Phys. 127 (2011) 137–142. doi:10.1016/j.matchemphys.2011.01.046.

[41]   J.A. Prince, G. Singh, D. Rana, T. Matsuura, V. Anbharasi, T.S. Shanmugasundaram, Preparation and characterization of highly hydrophobic poly(vinylidene fluoride) – Clay nanocomposite nanofiber membranes (PVDF–clay NNMs) for desalination using direct contact membrane distillation, J. Memb. Sci. 397-398 (2012) 80–86. doi:10.1016/j.memsci.2012.01.012.

[42]   L. Wang, C.-L. Pai, M.C. Boyce, G.C. Rutledge, Wrinkled surface topographies of electrospun polymer fibers, Appl. Phys. Lett. 94 (2009) 151916. doi:10.1063/1.3118526.

[43]   B.S. Lalia, E. Guillen-Burrieza, H. a. Arafat, R. Hashaikeh, Fabrication and characterization of polyvinylidenefluoride-co-hexafluoropropylene (PVDF-HFP) electrospun membranes for direct contact membrane distillation, J. Memb. Sci. 428 (2013) 104–115. doi:10.1016/j.memsci.2012.10.061.

[44]   D. Crespy, K. Friedemann, A.-M. Popa, Colloid-electrospinning: fabrication of multicompartment nanofibers by the electrospinning of organic or/and inorganic dispersions and emulsions., Macromol. Rapid Commun. 33 (2012) 1978–1995. doi:10.1002/marc.201200549.

[45]   A.M. Alklaibi, N. Lior, Membrane-distillation desalination: Status and potential, Desalination. 171 (2005) 111–131. doi:10.1016/j.desal.2004.03.024.

[46]   J. Phattaranawik, Effect of pore size distribution and air flux on mass transport in direct contact membrane distillation, J. Memb. Sci. 215 (2003) 75–85. doi:10.1016/S0376-7388(02)00603-8.

[47]   K.W. Lawson, D.R. Lloyd, Membrane distillation, J. Memb. Sci. 124 (1997) 1–25. doi:10.1016/S0376-7388(96)00236-0.

[48]   K.H. Lee, H.Y. Kim, Y.J. Ryu, K.W. Kim, S.W. Choi, Mechanical behavior of electrospun fiber mats of poly(vinyl chloride)/polyurethane polyblends, J. Polym. Sci. Part B Polym. Phys. 41 (2003) 1256–1262. doi:10.1002/polb.10482.

[49]   M. Essalhi, M. Khayet, Self-sustained webs of polyvinylidene fluoride electrospun nano-fibers: Effects of polymer concentration and desalination by direct contact membrane distillation, J. Memb. Sci. 454 (2014) 133–143. doi:10.1016/j.memsci.2013.11.056.

[50]   S. Roy, M. Bhadra, S. Mitra, Enhanced desalination via functionalized carbon nanotube immobilized membrane in direct contact membrane distillation, Sep. Purif. Technol. 136 (2014) 58–65. doi:10.1016/j.seppur.2014.08.009.

[51]   L.D. Tijing, Y.C. Woo, W.G. Shim, T. He, J.S. Choi, S.H. Kim, et al., Superhydrophobic

nanofiber membrane containing carbon nanotubes for high-performance direct contact membrane distillation, J. Memb. Sci. 502 (2016) 158–170. doi:10.1016/j.memsci.2015.12.014.

[52] X. Li, X. Yu, C. Cheng, L. Deng, M. Wang, X. Wang, Electrospun Superhydrophobic Organic/Inorganic Composite Nanofibrous Membranes for Membrane Distillation, ACS Appl. Mater. Interfaces. (2015) 150929124751008. doi:10.1021/acsami.5b06509.

[53] Z.-Q. Dong, X.-H. Ma, Z.-L. Xu, Z.-Y. Gu, Superhydrophobic modification of PVDF-SiO2 electrospun nanofiber membranes for vacuum membrane distillation, RSC Adv. 5 (2015) 67962–67970. doi:10.1039/C5RA10575G.

Table 1. Properties of PH ENMs incorporating TiO_2 nanoparticles.

Number	Membrane	Mean Pore size (µm)	Maximum size (µm)	Thickness (µm)	Porosity (%)	LEP (kPa)	Contact angle (°)	Fiber diameter (nm)	Tensile strength (MPa)	Elongation at break (%)
M-1	10%PH 1%TiO_2	0.3201	0.4069	89±7	88.9±1.1	122.5±1.5	145.0±1.1	135±36	6.5	63.9
M-2	10%PH 5%TiO_2	0.3335	0.4869	81±6	89.9±1.0	124.5±1.5	145.6±0.4	119±39	5.0	60.7
M-3	10%PH 10%TiO_2	0.3186	0.4801	92±2	90.2±1.3	194.5±1.5	148.0±0.7	141±42	6.8	78.7
M-4	15%PH 1%TiO_2	0.5706	0.7290	77±2	89.2±1.2	97.0±1.6	146.9±1.2	136±24	6.5	67.0
M-5	15%PH 5%TiO_2	0.6239	0.7726	83±2	89.6±1.2	113.3±3.7	146.2±0.6	138±50	5.7	69.5
M-6	15%PH 10%TiO_2	0.6229	0.7949	80±1	90.5±1.1	106.0±3.7	148.5±2.2	144±56	5.5	66.6
M-7	20%PH 1%TiO_2	0.7433	0.8840	97±7	88.8±0.9	93.6±0.3	146.8±1.0	280±94	6.8	128.7
M-8	20%PH 5%TiO_2	0.7332	0.8918	93±2	91.5±1.5	81.8±0.2	146.0±0.2	313±111	7.3	136.8
M-9	20%PH 10%TiO_2	0.7567	0.8701	100±8	91.6±1.6	96.3±1.7	149.0±2.8	296±74	7.0	124.9
M-N	Neat 20%PH	0.7613	0.8834	87±4	88.6±0.9	65.8±3.2	143.5±1.9	368±78	9.1	137.1

Table 2. Properties and DCMD performance between neat ENMs and ENMs incorporated with nano-filler. Feed/permeate temperature: 60/20°C. 3.5 wt% NaCl feed solutions except for our study (7.0 wt%)

Particle adding method	Material	Mean Pore size (μm)	Porosity (%)	Thickness (μm)	Contact angle (°)	Final flux (kg/m^2/h)	Operation time (h)	Permeate conductivity (μS/cm)
Surface coating	200% SiO$_2$-PVDF* [16]	0.32	80[+]	72	152.4	25	25	< 5
	PVDF [18]	0.68[a]	85	115	142.8	12.3	45	1.0→5.0
	200%SiO$_2$-PVDF*	0.69[a]	82	102	156.3	18.1	48	1.0→2.5
	PH [51]	0.58	89	82	149.0	22	5	0.5→13
	5%CNT-PH*	0.29	84	81	158.5	29.5	5	0.5→1.0
Mixing with dope solution	PVDF [52]	0.32	80.4	100	135.5	32.5	24	2.0→5.0
	222%SiO$_2$-PVDF	0.61	79.7	100	152.3	41.1	24	2.0→2.5
	PVDF[b] [53]	0.38	83	102	130.4	25.4	15	19.5→103
	27%SiO$_2$-PVDF[b]*	0.29	79	98	151.9	32.5	15	Not increase
	PH (our study)	0.76	88.6	87	143.5	33.4	48	0.9→83
	10%TiO$_2$-PH*	0.75	91.6	100	149.0	37.8	48	0.8→2.3

[a] Surface mean pore size based from the SEM images.

[b] Performance of vacuum membrane distillation.

* Concentration of additives (nano-filler) was based on weight of polymer.

[+] When authors didn't mentioned data values exactly, it was estimated from data graphs.
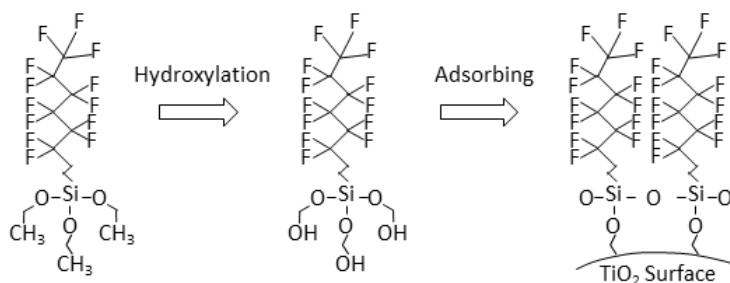
Fig. 1. Schematic representation of functionalized TiO$_2$ with FTES
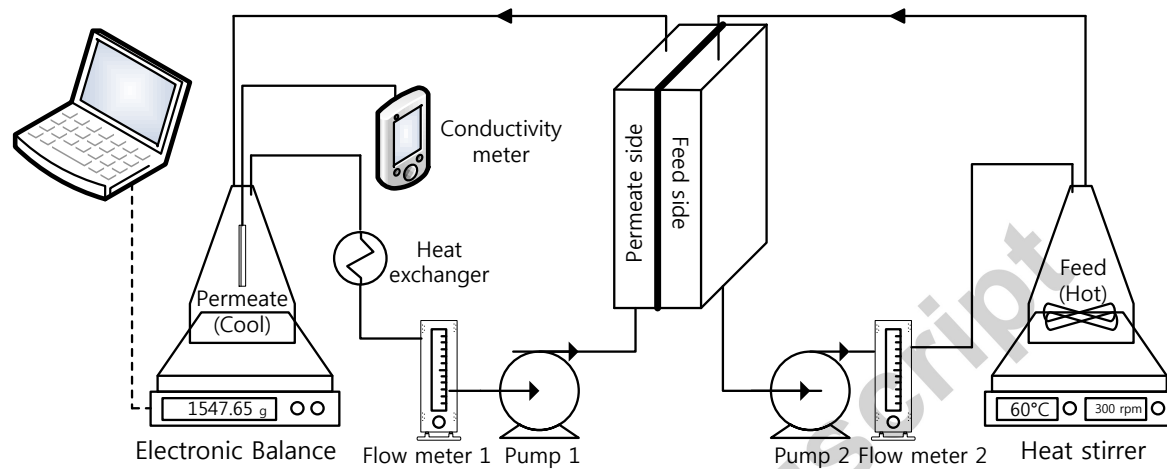
Fig. 2. Schematic diagram of the lab-scale DCMD system
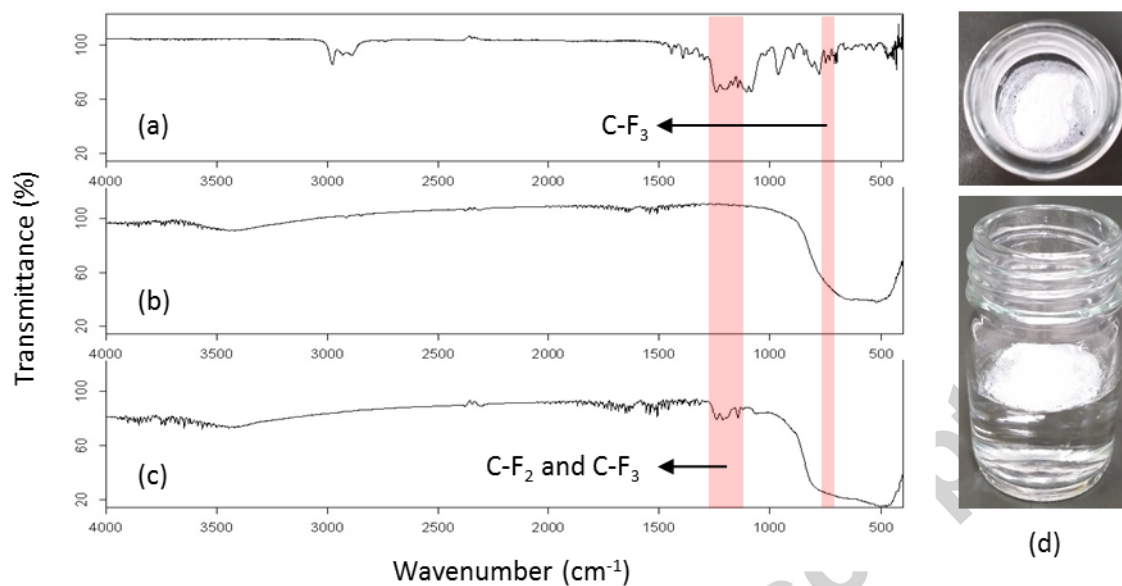
Fig. 3. FTIR spectra of (a) FTES, (b) pristine TiO_2 nanoparticles, and (c) functionalized TiO_2 nanoparticles. (d) Immiscible modified TiO_2 particles in distilled water.
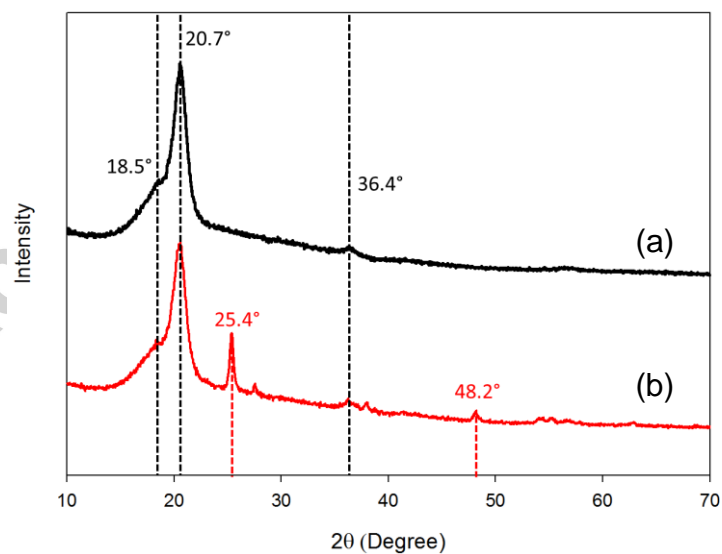
Fig. 4. XRD patterns of (a) neat 20% PH ENM and (b) 20% PH ENM containing 10% functionalized TiO_2 nanoparticles.
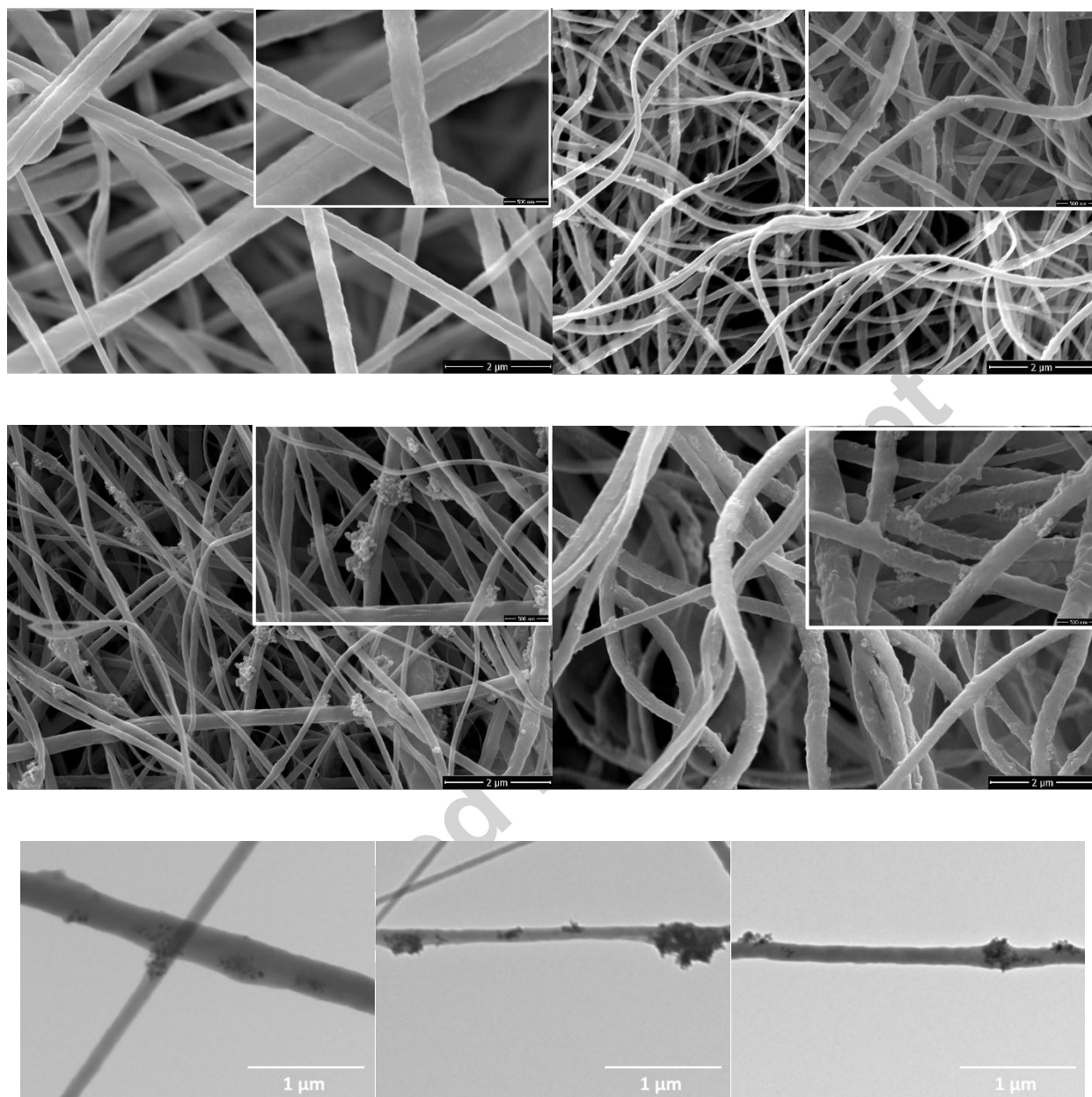
Fig. 5. FE-SEM images of (a) neat 20% PH ENM, (b) 10% PH ENM with 10% TiO_2, (c) 15% PH ENM with 10% TiO_2, and (d) 20% PH ENM with 10% TiO_2. TEM images of (e) 10% PH ENM with 10% TiO_2, (f) 15% PH ENM with 10% TiO_2, and (g) 20% PH ENM with 10% TiO_2
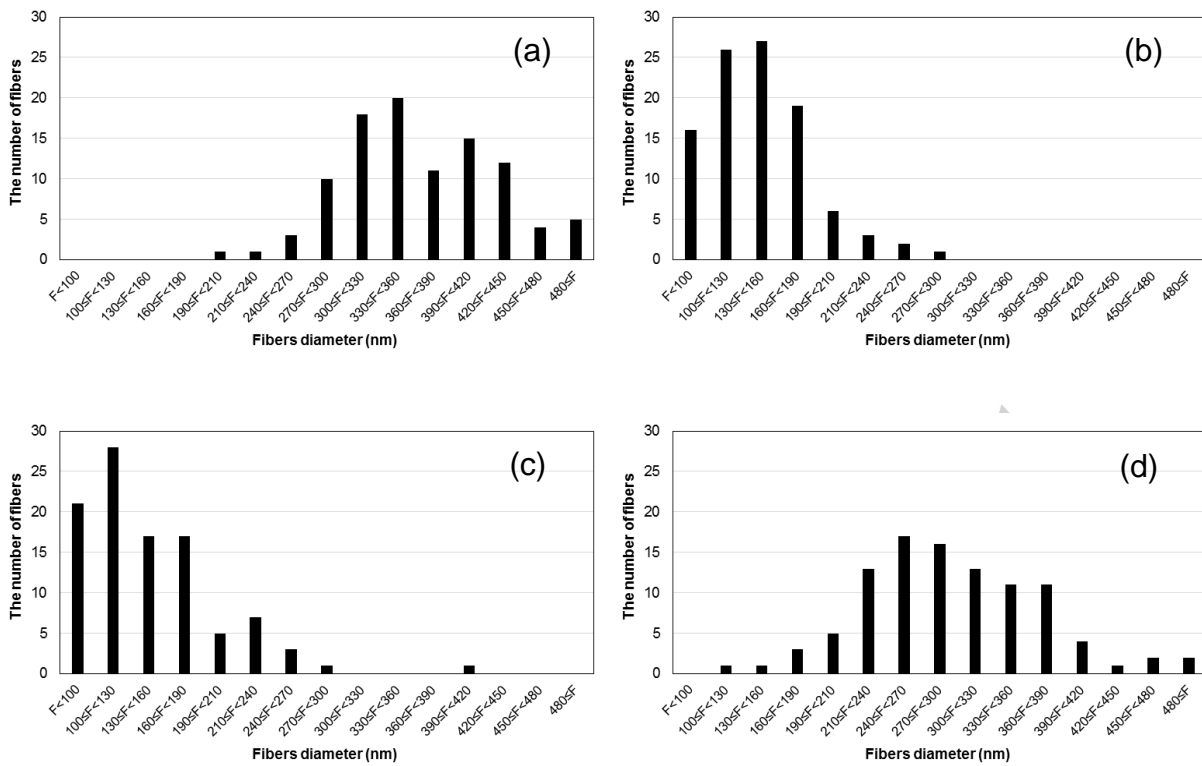
Fig. 6. Fiber diameter distributions of (a) neat 20% PH ENM, (b) 10% PH ENM with 10% TiO_2,

(c) 15% PH ENM with 10% TiO_2, and (d) 20% PH ENM with 10% TiO_2.
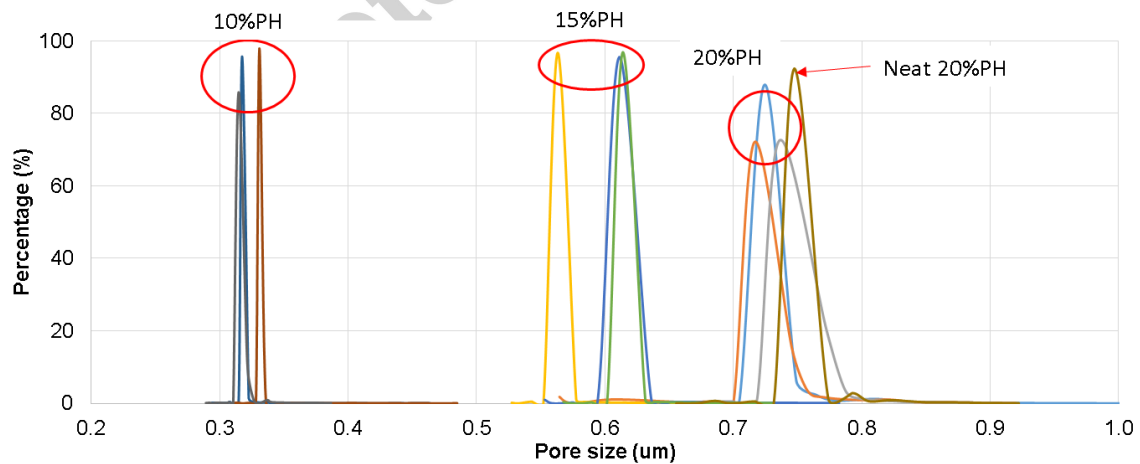
Fig. 7. Pore size distributions of the neat PH ENM and PH ENMs containing TiO_2 nanoparticles.
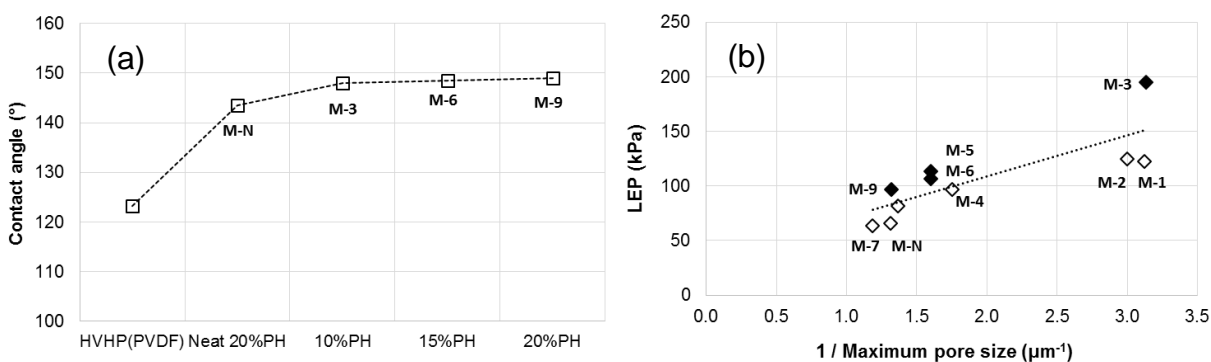
Fig. 8. (a) Contact angle and (b) LEP of electrospun membrane incorporating TiO$_2$ nanoparticles.
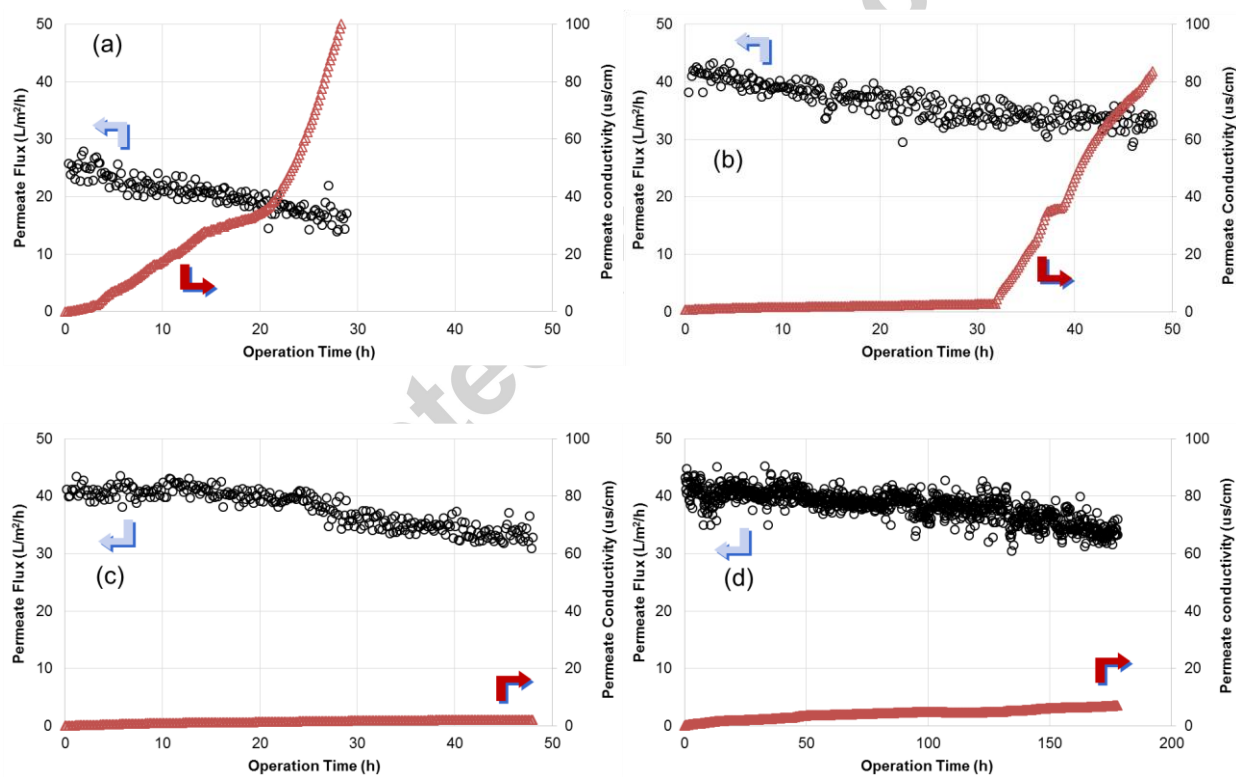
Fig. 9. DCMD performance of (a) commercial PVDF (0.45μm), (b) neat 20% PH ENM, (c) 10% PH ENM with 10% TiO$_2$, and (d) 20% PH ENM with 10% TiO$_2$.

Graphical abstract
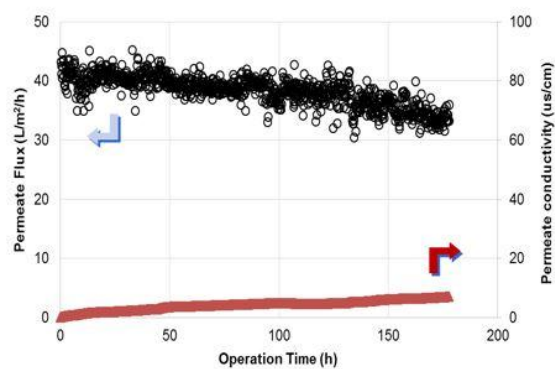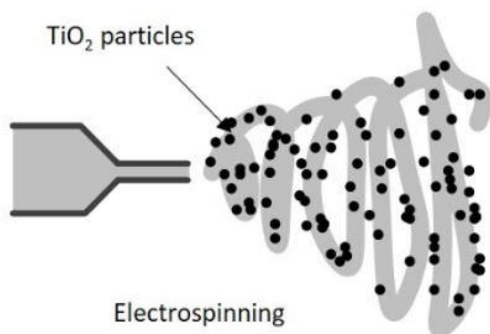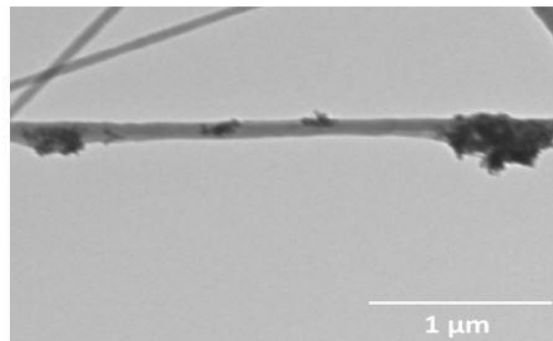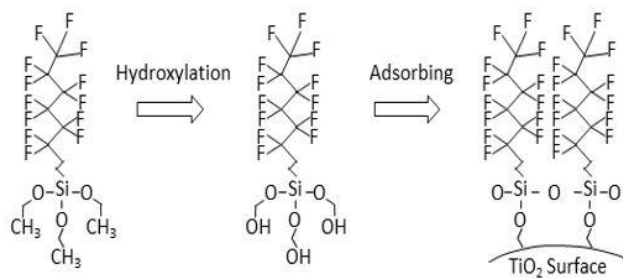
Highlights

- The fabrication of ENMs with addition of modified TiO_2 particle to dope solution for MD
- The effect of hydrophobic TiO_2 nanoparticle embedded in fibers on properties of ENMs
- Improved ENMs with 149° of contact angle or 194.5 kPa of LEP by addition of 10% TiO_2
- The evaluation of DCMD performance with functionalized ENMs by TiO_2 particles
- DCMD without deterioration of water productivity and quality in 20% PH with 10% TiO_2